Supporting Information

Chiu *et al.* 10.1073/pnas.0804610105

SI Text

Mice and Symptomatic Analysis. B6/SJL F1 SOD1^{G93A} Tg, SOD1^{WT} Tg, and Non-Tg mice were purchased from the Jackson Laboratories Mice were analyzed at day 65 (presymptomatic), day 100 (early symptomatic), and day 135 (late symptomatic/end-stage) time points. Disease end-stage was determined by symptomatic progression and animal care guidelines (therefore at times varying from the day 135 time-point by ± 5 days). B6 congenic SOD1^{G93A} Tg mice were obtained from the Jackson Laboratory. A substrain expressing lower copy number of the mutant SOD1 transgene (survival occurring approximately 30 days later than the B6 high copy strain) were received from the Jackson Laboratory and used to establish our animal colony. To generate mutant SOD1 mice deficient in T lymphocytes, B6.SOD1^{G93A} Tg males were bred with B6.TCRβ−/− females; Resulting B6.SOD1^{G93A} Tg TCRβ+/- F1 males were recrossed to B6.TCRβ−/− females. F2 generation B6.SOD1^{G93A}Tg TCRβ+/- and B6.SOD1^{G93A}Tg TCRβ−/− littermates were used for analysis. Mutant SOD1 expression levels were assayed as equivalent between SOD1^{G93A}Tg TCRβ +/+, TCRβ+/-, and TCRβ−/− animals by quantitative PCR analysis for human SOD1 (see primers below). Mice were confirmed to be $\alpha\beta$ T cell deficient by PCR genotyping using primers 5′TGTCTGAAGGGCAATGACTG3′, 5′GCTGATCCGTGGCATCTAAT3′, and 5′TATTGGCTGCAGGTCGAAAG3′, and by FACS analysis for CD4, CD8, and TCRbeta. Disease progression was documented according to previously established methodology. Symptomatic analysis was conducted by daily monitoring and weight measurements every 4–5 days starting at day 90. Symptomatic onset was defined as the age at which animals reached maximum weight (1, 2). In conjunction, animals were scored for motor symptoms using the following criteria: 7 = no symptoms, 6 = hind-limb spread reflex noticeably affected when lifted by tail, 5 = hind-limbs show tremors when lifted, 4 = noticeable decrease in size/weight and gait abnormalities, 3 = moderate symptoms of hind-limb paresis and moderate gait abnormalities, 2 = paralysis of both hind-limbs but able to move about with forelimbs, 1 = End-stage, inability of animal to right itself after 15 sec; euthanasia. We used peak weight as an objective method of determining disease onset (1, 2). In Fig. 6, the early symptomatic phase was defined as time between disease onset (peak weight) to 5% drop in weight; late symptomatic phase as between 5% drop in weight and end-stage. Animal protocols were approved by Institutional Animal Care and Use Committee (IACUC) at Harvard Medical School and are according to NIH guidelines.

Flow Cytometry. Microglia and T cells were directly isolated from the CNS of mice as described (3–5). Mice were transcardially perfused with ice cold phosphate-buffer saline (PBS), spinal cords and brains separately dissected. Single cell suspensions were prepared and centrifuged over a 37%/70% discontinuous Percoll gradient (GE Healthcare), immune cells isolated from the interface, and total cell count determined. Cells were preblocked with anti-CD16/CD32 (Fc Block), and stained on ice for 30 min with combinations of anti-CD45-FITC, anti-MHC class II-FITC (clone NIMR-4), anti-CD86 Biotin, anti-CD80 Biotin, anti-TCRβ-APC, anti-NK1.1-APC (from eBioscience), anti-CD3ε Biotin, anti-CD11c-FITC, anti-CD69-FITC, anti-CD44-FITC, anti-CD19-PE, anti-CD54-PE, anti-CD11b-PE, anti-CD4-PercP, anti-CD8-PercP, anti-TCR$\gamma\delta$-PE, anti-CD11b-APC, rat IgG isotype controls (from BD Biosciences) and in some stains followed by Streptavidin-APC (BD Biosciences). Appropriate antibody IgG isotype controls (BD Biosciences) were used for all stains. Four color fluorescence activated cell sorting (FACS) analysis was performed on a FACScalibur machine (BD Biosciences), and data subsequently analyzed with FlowJo Software (TreeStar Software).

Microglia Magnetic Bead Purification. Spinal cord or brain immune cells isolated by 37%/70% Percoll gradient were subjected to CD11b magnetic bead selection to specifically purify microglia. Cells were incubated with CD11b magnetic beads (Miltenyi Biotech) for 15 min at 4 °C, and run over MS selection columns per manufacturer's instructions (Miltenyi Biotech). To check selection purity, samples were stained postselection with CD11b and CD45 and analyzed by flow cytometry (Fig. S6). Microglia were centrifuged and immediately resuspended in TRIzol reagent (Invitrogen) for RNA purification and expression analysis. Microglia isolated by such methodology reflects *in vivo* gene expression (6).

Primary Adult Microglia Culture and Stimulation. For expansion of primary adult microglia, we followed protocols described by Ponomarev *et al.* with minor modifications (7). Immune cells were isolated by 30%/70% Percoll gradient from CNS of 7 week old SOD1^{G93A} Tg or non-Tg mice, washed twice with Hanks Buffered Saline Solution (HBSS)/2% Fetal Calf Serum (FCS), and seeded in 24 well plates after resuspension in Dulbecco's Modification of Eagle's Medium (Invitrogen)/10% FCS, 50 μM 2-Mercaptoethanol, 2 mM L-Glutamine, Penicillin/Streptomycin supplemented with 10 ng/ml M-CSF (Peprotech). Media was changed every 3 days while microglia grew in culture. After 2 weeks, microglia were gently removed by non-enzymatic cell dissociation solution in HBSS (Sigma), and replated in 24 well plates at 2×10^4 cells/well with 20 ng/ml IL-4 or 50 ng/ml IFN-γ. After 3 days, cells were subjected to flow cytometry or resuspended in TRIzol Reagent (Invitrogen) for quantitative PCR.

N9 Microglia Culture, Viral Transduction and Cytokine Stimulation. The N9 microglia cell line (8, 9) was kindly gifted by Dr. Laura Santambrogio (Albert Einstein School of Medicine, New York, NY). N9 cells were cultured in DMEM/10%FCS/2 mM L-Glutamine/Penicillin/Streptomycin. Recombinant lentiviral constructs were engineered to over-express SOD1^{WT} or SOD1^{G93A}. Human SOD1^{WT} and SOD1^{G93A} were subcloned into a lentiviral vector driven by fEF1alpha promoter, kindly provided by Dr. Jeng-Shin Lee (Harvard Gene Therapy Initiative, Boston, MA). 293T cells (Invitrogen) were cotransfected with human SOD1^{WT}, SOD1^{G93A} or empty vector together with the commercial lentiviral packaging plasmids pLP1 (gag/pol), pLP2(rev), and pLP/VSVG (VSV-G env) using Lipofectamine 2000 (Invitrogen). Media was changed at 24 h, viral particles harvested at 48 h, passaged through 40 μm filters and stored at −80 °C until use. For transduction, N9 cells were plated in 24 well plates at 2×10^5 cells/well, 500 μl viral supernatant added with 4 μg/ml Polybrene (Sigma), followed by centrifugation at 2500 rpm for 90 min at 30 °C. Fresh culture media was added immediately following spin infection. At 48 h following transduction, N9 cells were replated at 2×10^5 cells/well and either untreated or stimulated with 20 ng/ml IL-4 overnight. Cells were lysed in TRIzol (Invitrogen), RNA extracted, and cDNA synthesized using the iScript synthesis kit (Bio-Rad). Real-time PCR was used to analyze cytokine induced gene expression.

ELISpot Analysis. Microglia and T cells were isolated by 37%/70% Percoll gradient from spinal cords or brains of end-stage day 135 B6SJL SOD1^{G93A} Tg mice or littermate Non-Tg mice. Cells were plated at 2×10^4 cells/well and cultured in the presence or absence of 4 μg/ml Con A (Sigma) for 48 h. IL-4 ELISpot development was performed using an IL-4 ELISpot kit per manufacturer's instructions (BD Biosciences). Positive spots were counted by ELISPot plate reader (ImmunoSpot).

Tissue Processing, Immunofluorescence, and Image Analyses. Mice were transcardially perfused with ice-cold PBS, followed by 4% paraformaldehyde (PFA)/PBS. Spinal cords were dissected and postfixed overnight in 4% PFA/PBS, infiltrated with 10% and 30% sucrose, and embedded into Optimal Cutting Temperature (OCT, Tissue Tek). Cryosections were cut at 15 μm thickness and stored at -20 °C until use. For immunostaining, sections were rehydrated in PBS, blocked for 2 h. at room temperature (RT) and stained in PBS/5% goat serum/0.1% Tween 20. Primary antibody was incubated overnight at 4 °C, and followed by secondary antibody for 1 h at room temperature. Stained sections were mounted in fluorescence media with DAPI (Vector Labs) and imaged using a Bio-Rad Radiance 2000 MP laser scanning confocal microscope (Bio-Rad). To detect dendritic cells, hamster anti-mouse CD11c (1:50, clone HL3, BD Biosciences) was followed by Cy3 goat-anti-hamster IgG (Jackson Immunoresearch). To detect microglia, rat anti-mouse CD68 (1:500, AbD Serotec) or rat anti-mouse CD11b (1:100, clone M1/70, BD Biosciences) was followed by Alexa 488 anti-rat IgG (Invitrogen). To detect astrocytes, rabbit anti-GFAP (1:1000, Sigma) was followed by Alexa 488 goat anti-rabbit IgG (Invitrogen). Staining for IGF-1 was based on protocols established by Lalancette *et al.*, 2007 (10); sections were stained with IGF1 monoclonal antibody, clone Sm1.2 (1:100, Millipore), followed by Alexa 568 goat anti-mouse IgG (Invitrogen). We used Metamorph Imaging software (Molecular Devices) for image analysis. For pixel quantification, serial lumbar spinal cord sections were imaged; fields used for analysis were 210 μm $\times$ 210 μm. Red and green staining were segmented and measured for total positive staining area. For segmentation, a threshold value of 65/255 was used in Metamorph; threshold positive pixels in both green and red channels were determined as co-localized. Integrated intensity is defined as the intensity of all pixels integrated over the entire area (MetaMorph).

Immunohistochemistry and Histopathology. Mice were transcardially perfused with 4% PFA/PBS, spinal cords dissected, infiltrated with 10% and 30% sucrose, embedded into OCT, and frozen. 30 μm free-floating cryosections were cut from lumbar spinal cord. For immunohistochemistry, endogenous peroxidase activity was quenched with 0.3% hydrogen peroxide for 20 min at RT. Sections were preblocked in PBS/0.3% Triton-X/5% goat serum/1% BSA, and incubated overnight at 4 °C with rabbit anti-Iba1 (1:500, Wako Chemicals), followed by biotin goat anti-rabbit IgG (1:500, Jackson Immunoresearch) for 2 h at RT. Antibody was detected using the Vectastain ABC Peroxidase kit according to manufacturer's instructions (Vector Labs) and 3,3′-Diaminobenzidine (DAB) substrate (Vector Labs). Sections were transferred to slides, dried overnight, dehydrated, cleared in xylenes, and mounted in Permount (Fisher Scientific).

Neuronal histopathology was analyzed at day 140 and end-stage time-points for non-Tg, TCR$-/-$, SOD1^{G93A}, and SOD1^{G93A} TCR$-/-$ mice (n = 2–4 as indicated in Fig. S13). Mice were transcardially perfused with 4% PFA/PBS, spinal cord dissected, and embedded into OCT. 30 μm sections were cut from lumbar spinal cord, skipping every other section, and adhered onto Superfrost Plus Slides (Fisher Scientific). Lumbar sections were stained for 5 min with 0.1% Thionin solution (Sigma), differentiated in 95% ETOH and glacial acetic acid, dehydrated, cleared in xylenes, and mounted in Permount (Fisher Scientific). We examined 5–15 non-consecutive Nissl-stained lumbar sections per individual animal and images were taken of ventral horn areas of each section (left and right) at 20× magnification. NIH Image J software was used for morphometric analysis and neuronal counting. Motor neurons were defined as Nissl positive cells with distinct nuclei and area >250 μm^2; average motor neuron counts/field were established for individual animals and confirmed by a blinded observer.

Microarray Analysis Criteria. Data were collected from Mouse 430 2.0 microarray GeneChips (Affymetrix) by Affymetrix Microarray Suite 5.0 software (Dana Farber Gene Chip Facility). Subsequent analysis was carried out using dCHIP software (11). Results were normalized and model-based expression values calculated using the probe match/mismatch model. Sample comparisons were conducted using the following criteria:

For Table S2, selection criteria included presence call of 100%, minimal lowest fold change of >10.0 for increased expression, and >7.0 for decreased expression at the late symptomatic time point, and signal differences >100.

For Table S3, ontologically classified lists based on functional annotations (Affymetrix) were generated, followed by comparison analysis and selection for genes with >2.00 fold changes at either time point (100% present). Of these, selected gene families with highly regulated expression changes are listed.

For Table S4 and Table S5, changes in gene expression for early symptomatic and late symptomatic time points are listed. Genes were selected with >2 fold expression changes (100% present) and listed in descending order from most significant increase to most significant decrease.

Real-Time PCR Primers and Conditions. Quantitative real-time PCR reactions were carried out using SYBR green incorporation with gene specific primers. Relative gene expression was calculated by $\Delta\Delta$ cT analysis relative to GapdH expression levels. Real-time PCR primer sequences used were,

IGF-1: 5′ CTGGACCAGAGACCCTTTG 3′ and 5′ CCTGTGGGCTTGTTGAAGTAAAA 3′; SOD1: 5′ AGGGCATCATCAATTTCGAGC 3′ and 5′ GCCCACCGTGTTTCTGGA 3′; CD11c: 5′ ACACAGTGTGCTCCAGTATGA 3′ and 5′ GCCCAGGGATATGTTCACAGC 3′, IL-6: 5′ TCCAGTTGCCTTCTTGGGAC 3′ and 5′ GTGTAATTAAGCCTCCGACTTG 3′; Osteopontin: 5′ AGCAAGAAACTCTTCCAAGCAA 3′ and 5′ GTGAGATTCGTCAGATTCATCCG 3′; Matrix Metalloproteinase 12 (MMP-12): 5′ GAGTCCAGCCACCAACATTAC 3′ and 5′ GCGAAGTGGGTCAAAGACAG 3′; Cholesterol 25-Hydroxylase: 5′ TGCTACAACGGTTCGGAGC 3′ and 5′ AGAAGCCCACGTAAGTGATGAT 3′; Apolipoprotein CII: 5′ ACCTGTACCAGAAGACATACCC 3′ and 5′ GTAAAAATGCCTGCGTAAGTGC 3′; IL-1 Receptor Antagonist: 5′ GCTCATTGCTGGGTACTTACAA 3′ 5′ CCAGACTTGGCACAAGACAGG 3′ Gapdh: 5′ TGGCAAAGTGGAGATTGTTGCC 3′ and 5′ AAGATGGTGATGGGCTTCCCG 3′. For TNF-α, commercial primers were used (quantitect, Qiagen). Primer design was based on literature (12) or by the real-time primer bank (http://pga.gh.harvard.edu/primerbank) (13). All reactions were verified for specificity by melting curve analysis and 1.5% agarose gel electrophoresis. For all SYBR green reactions, the Perfect Real-time Ex Taq mix (Takara Mirus Bio) was used, and run on an iCycler iQ machine (Bio-Rad) using the following amplification conditions: i) 94 °C for 3 min and ii) 94 °C for 15 seconds followed by 60 °C for 45 seconds for 40 cycles.

T Cell Deficiency Directly Affects CNS Pathology and Does Not Lead to Confounding Peripheral Defects. One specific concern was that TCRβ deficiency would cause confounding non-neurological

defects, leading to acceleration of phenotype in mutant SOD1 mice. The following data addressed this concern:

i) Absence of T lymphocytes led to unequivocal and direct effects on CNS pathology, which was specific to SOD1^{G93A} TCR$\beta-/-$ animals and not in TCR$\beta-/-$ animals. In particular, survival of spinal cord motor neurons and microglia activation were directly affected in the CNS.

a) The morphological activation of microglia, as determined by immno-staining for CD68 (Fig. 5*A*), CD11b, CD11c (Fig. 5*B* and Fig. S11), and Iba1 (Fig. S12) were significantly diminished in spinal cords of SOD1^{G93A}TCR$\beta-/-$ compared to SOD1^{G93A} Tg mice. Furthermore, microglia expression of IGF-1, a motor neuron protective factor, was largely reduced in SOD1^{G93A} TCR$\beta-/-$ spinal cord sections (Fig. 5*B*).

b) Motor neuron pathology was significantly accelerated by the absence of T cells in SOD1^{G93A} Tg mice. Histopathology analysis showed a significant reduction of Nissl positive ventral horn motor neurons at day 140 in SOD1^{G93A} TCR$\beta-/-$ mice relative to SOD1^{G93A} mice (Fig. S13). By end-stage disease, motor neuron loss was equivalently in both lines. We note that CNS pathology was absent in non transgenic TCR$\beta-/-$ mice (Fig. S13). Therefore, T cell deficiency caused specific and direct effects on motor neuron death and microglia responses in mutant SOD1 mice.

ii) Systematic analysis shows that accelerated disease progression was not caused by peripheral defects related to T cell dysfunction.

a) TCR$\beta-/-$ littermate mice were included at every phase of experimental analysis. TCR$\beta-/-$ control mice did not display mortality (Fig. 6*A*), motor symptoms, motor neuron loss (Fig. S13) or weight loss (Fig. S10). TCR$\beta-/-$ animals gained weight during aging, similarly to wild-type C57/BL6 mice, which is in contrast with mutant SOD1 transgenic mice. Therefore, the absence of $\alpha\beta$ T cells alone does not lead to morbidity or mortality due to confounding peripheral defects.

b) In a past study, it has been shown that T cell receptor deficient mice can spontaneously develop inflammatory bowel disease (IBD). Mombaerts *et al.*(14) included RAG$-/-$, TCR$\delta-/-$, TCR$\alpha-/-$, and TCR$\beta-/-$ animals in their analysis. Notably, TCR$\alpha-/-$ mice were shown to have a much higher prevalence for IBD than TCR$\beta-/-$ mice in this analysis. All observed cases of IBD in TCR$\beta-/-$ mice occurred late in life ($>$ 6 months of age), and the authors noted that IBD depended on specific maintenance conditions of the animal facility used. All breeding and analysis for our current study was conducted before 7 months of age, and animals were maintained in a routinely screened, full barrier pathogen-free facility (Harvard Medical School, Warren Alpert Building).

We also systematically and routinely checked our animals for signs of IBD. After 90 days of age, biweekly observational checks were conducted for ano-rectal prolapse and chronic diarrhea (14). At necropsy following euthanasia, small and large intestines were examined for intestinal inflammation; IBD was not detected in the animals, including all B6.SOD1^{G93A}Tg TCR$\beta-/-$ or TCR$\beta-/-$ used for this study, based on the absence of anorectal prolapse, chronic diarrhea, and intestinal inflammation. TCR$\beta-/-$ animals did not display early mortality (Fig. 6*A*), and exhibited normal weight gain (Fig. S10), contrary to an IBD phenotype. Based on these cumulative data, we conclude that deficiency of TCRβ causes direct effects on pathology in the CNS of SOD1^{G93A} Tg mice, and that acceleration of disease was not due to other confounding, non-neurological defects in the periphery.

1. Boillee S, *et al.* (2006) Onset and progression in inherited ALS determined by motor neurons and microglia. *Science* 312:1389–1392.
2. Yamanaka K, *et al.* (2008) Astrocytes as determinants of disease progression in inherited amyotrophic lateral sclerosis. *Nat Neurosci* 11:251–253.
3. El Khoury J, *et al.* (2007) Ccr2 deficiency impairs microglial accumulation and accelerates progression of Alzheimer-like disease. *Nat Med* 13:432–438.
4. Ponomarev ED, Shriver LP, Maresz K, Dittel BN (2005) Microglial cell activation and proliferation precedes the onset of CNS autoimmunity. *J Neurosci Res* 81:374–389.
5. Sedgwick JD, *et al.* (1991) Isolation and direct characterization of resident microglial cells from the normal and inflamed central nervous system. *Proc Natl Acad Sci USA* 88:7438–7442.
6. De Haas AH, Boddeke HW, Brouwer N, Biber K (2007) Optimized isolation enables *ex vivo* analysis of microglia from various central nervous system regions. *Glia* 55:1374–1384.
7. Ponomarev ED, Novikova M, Maresz K, Shriver LP, Dittel BN (2005) Development of a culture system that supports adult microglial cell proliferation and maintenance in the resting state. *J Immunol* Methods 300:32–46.
8. Franco L, *et al.* (2006) Cyclic ADP-ribose is a second messenger in the lipopolysaccharide-stimulated activation of murine N9 microglial cell line. *J Neurochem* 99:165–176.
9. Li Y, *et al.* (2000) Neuronal-glial interactions mediated by interleukin-1 enhance neuronal acetylcholinesterase activity and mRNA expression. *J Neurosci* 20:149–155.
10. Lalancette-Hebert M, Gowing G, Simard A, Weng YC, Kriz J (2007) Selective ablation of proliferating microglial cells exacerbates ischemic injury in the brain. *J Neurosci* 27:2596–2605.
11. Lin M, *et al.* (2004) dChipSNP: Significance curve and clustering of SNP-array-based loss-of-heterozygosity data. *Bioinformatics* 20:1233–1240.
12. Butovsky O, *et al.* (2006) Glatiramer acetate fights against Alzheimer's disease by inducing dendritic-like microglia expressing insulin-like growth factor 1. *Proc Natl Acad Sci USA* 103:11784–11789.
13. Wang X, Seed B (2003) A PCR primer bank for quantitative gene expression analysis. *Nucleic Acids Res* 31:e154.
14. Mombaerts P, *et al.* (1993) Spontaneous development of inflammatory bowel disease in T cell receptor mutant mice. *Cell* 75:274–282.

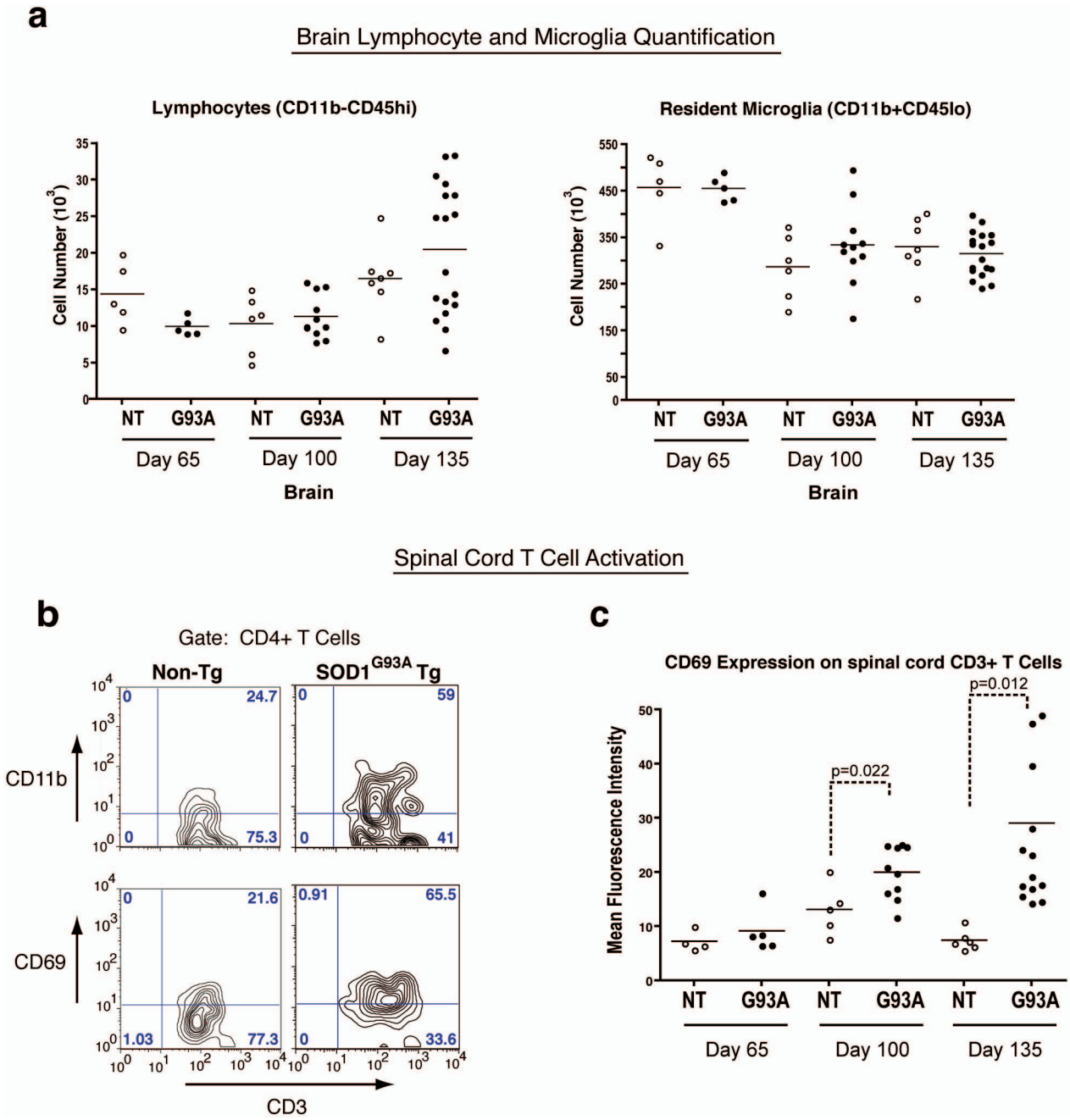

Fig. S1. Brain immune population dynamics and spinal cord T cell activation. (*a*) Brain immune cells isolated from SOD1^{G93A} Tg (G93A) or non-Tg (NT) mice were costained for CD11b and CD45 (as in Fig. 1) at day 65, day 100, and day 135. Lymphocytes (CD11b-CD45hi) and resident microglia (CD11b+CD45lo) were quantified as the product of total cell count by hemocytometer, and population percentage by FACS. (*b*) Spinal cord CD4$^+$ T cells were analyzed for the expression of CD3 (*x* axis) and activation markers CD11b or CD69 (*y* axis). All CD4$^+$ cells are positive for pan T cell marker CD3. CD69 and CD11b levels are higher on the CD4$^+$ T cell population from SOD1 ^{G93A} compared to non-Tg mice (*c*) Comparative analysis of CD69 levels on total spinal cord CD3+ T cells over the course of disease. Statistics by student's *t* test.

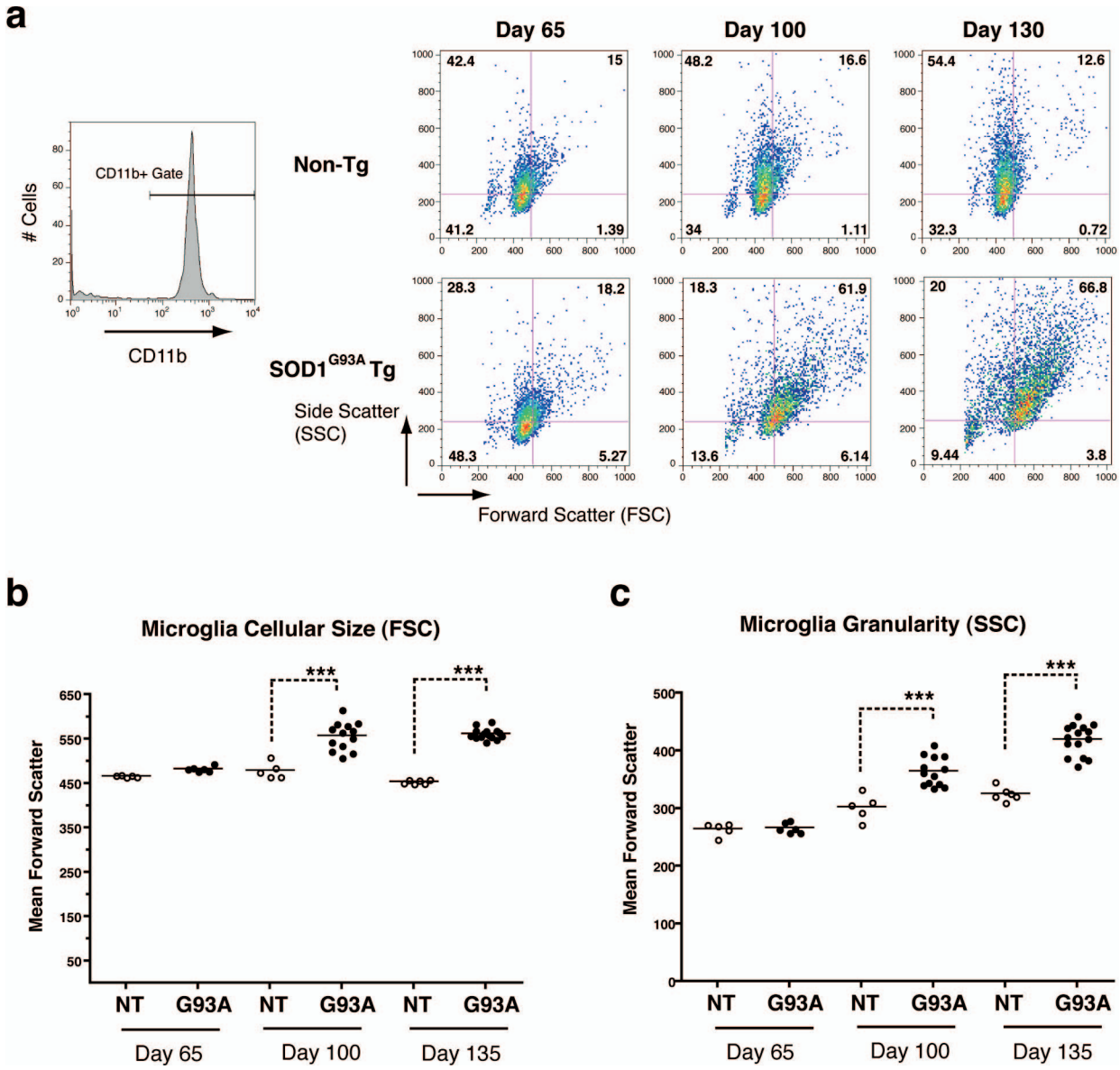

Fig. S2. Increased cell size and granularity of microglia in SOD1 ^{G93A} Tg mice. Spinal cord cells from non-Tg or SOD1 ^{G93A} mice were analyzed by flow cytometry. (*a*) Representative FACS plots of forward scatter (FSC) versus side scatter (SSC) properties of microglia. The CD11b+ gate for microglia is shown. (*b*) Quantification of the FSC (cell size) and SSC (granularity) properties of non-Tg (NT) and SOD1 ^{G93A} (G93A) microglia from individual mice at each time point. As seen, forward and side scatter of SOD1 ^{G93A} microglia increase significantly during disease. ***, $P < 0.001$ by *t* test.

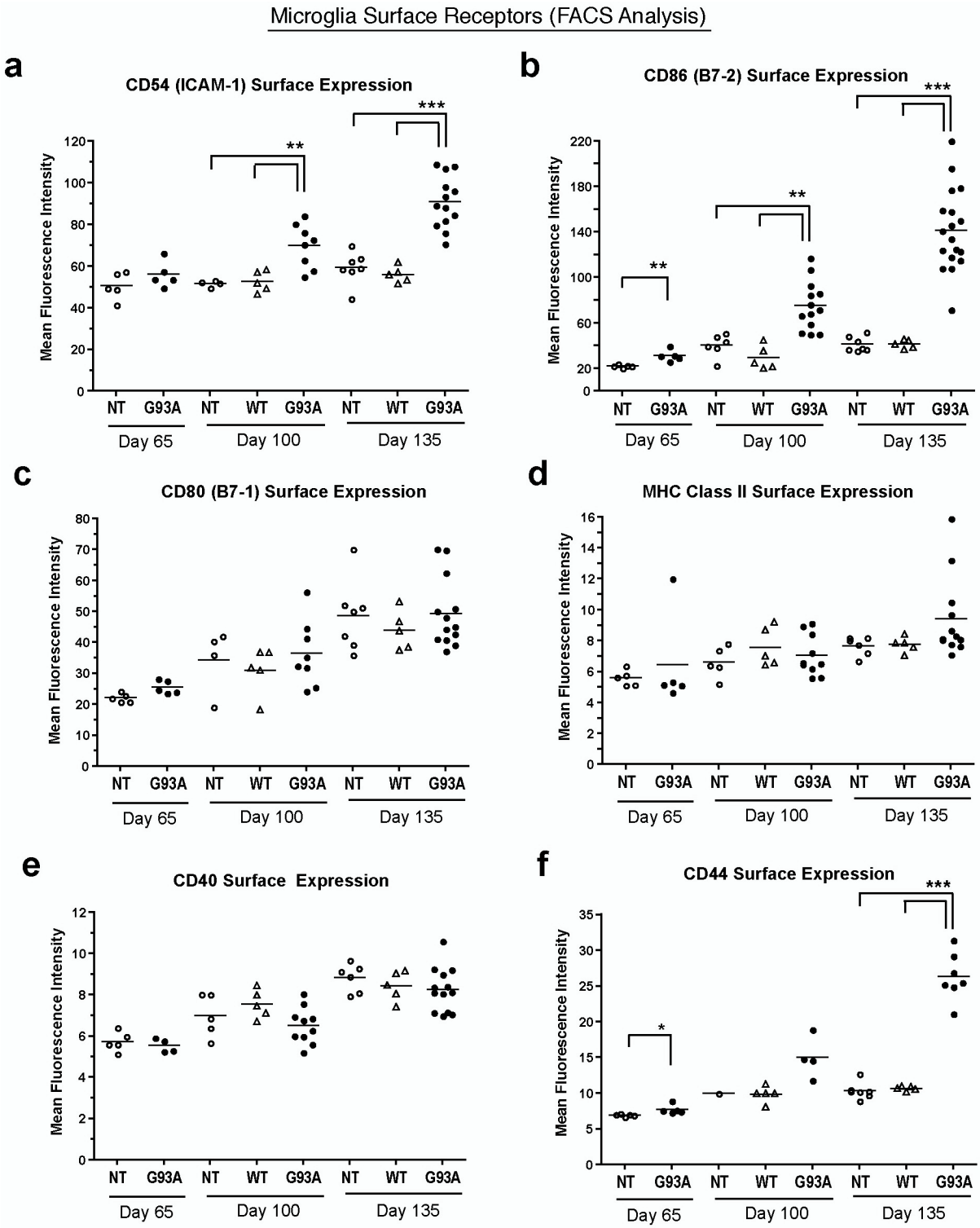

Fig. S3. Increased surface levels of CD86 (B7–2), CD54 (ICAM-1) and CD44, but not APC maturation markers on mutant SOD1 microglia. FACS analysis was conducted on percoll gradient isolated immune cells from spinal cords of non-Tg (NT), $SOD1^{WT}$ (WT) or $SOD1^{G93A}$ (G93A) mice at day 65, day 100, and day 135. Microglia (CD11b+) were gated on for mean fluorescence intensities of surface levels of the following receptors: (*a*) CD86 (B7–2) (*b*) CD54(ICAM-1) (*c*) CD80 (B7–1) (*d*) MHC class II (*e*) CD40 and (*f*) CD44 (osteopontin receptor). Statistical analysis (day 65, by *t* test, *, $P < 0.05$; day 100 and day 135, by One-way ANOVA with Boneferroni's post hoc test, **, $P < 0.01$ and ***, $P < 0.001$).

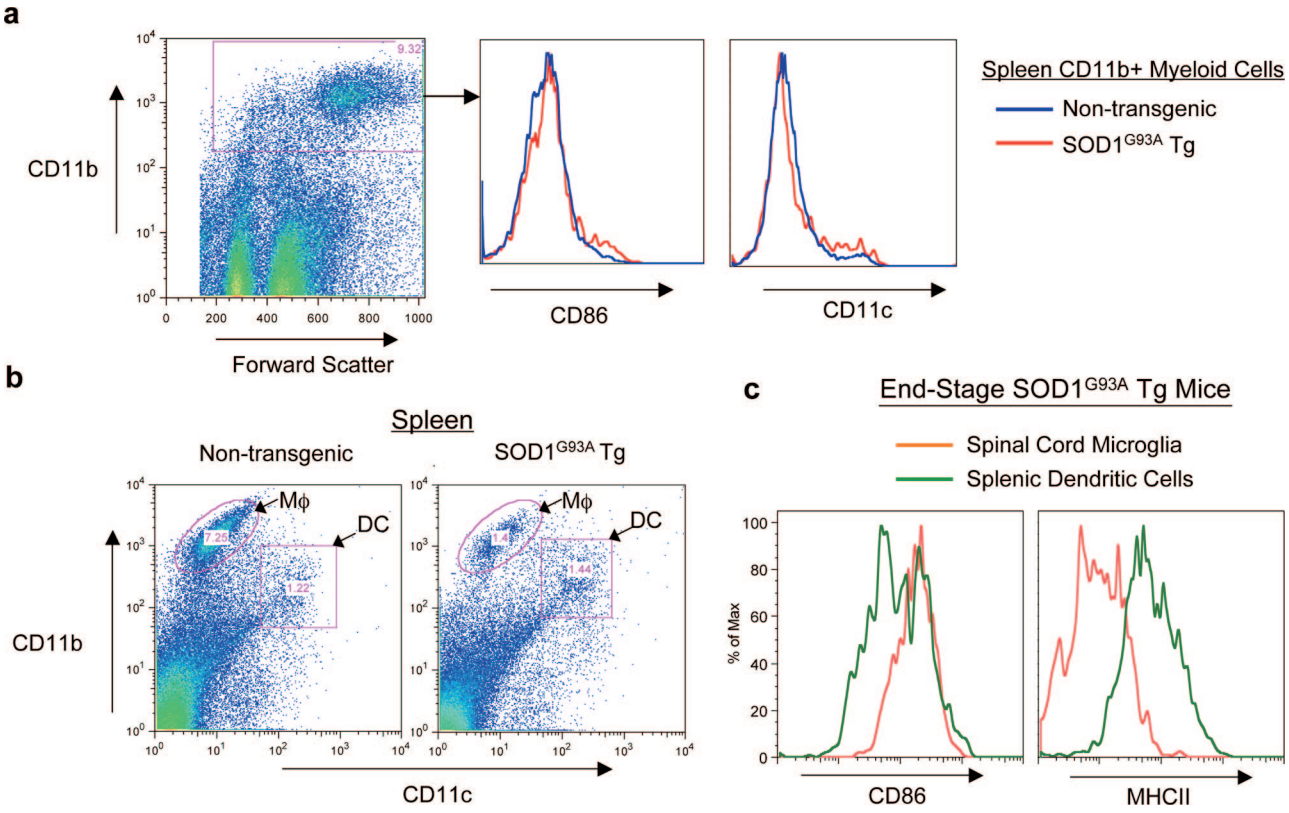

Fig. S4. Peripheral myeloid cells are not phenotypically equivalent to microglia in SOD1^{G93A} mice. (*a*) Total splenic CD11b+ cells showed equivalent levels of CD11c and CD86 (B7–2) in SOD1^{G93A} mice at end-stage compared to non-Tg littermates. (*b*) Macrophage (φ) and Dendritic cell (DC) populations in non-Tg and SOD1^{G93A} spleens. While the DC population is unchanged, Mφ population is reduced in mutant SOD1 mice. (*c*) Direct comparison of surface levels of CD86 and MHC class II on spinal cord microglia and splenic dendritic cells from the same SOD1^{G93A} animal (end-stage). Data are representative of >5 animals analyzed.

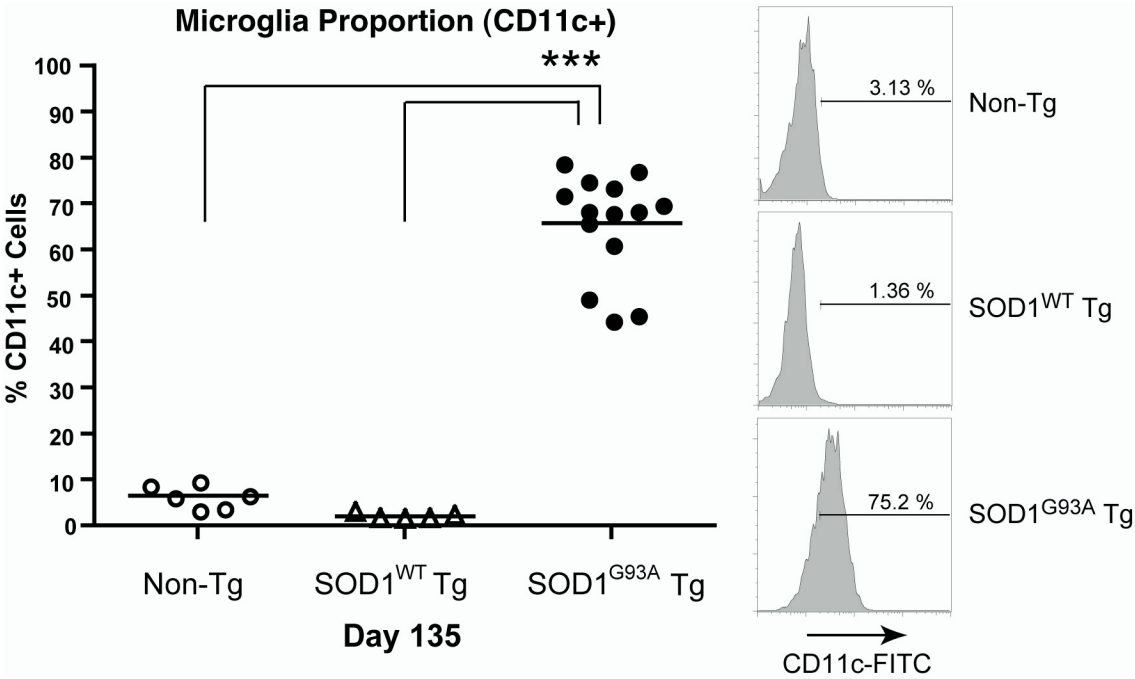

Fig. S5. The majority of microglia acquire CD11c expression. Microglia isolated from spinal cords of $SOD1^{G93A}$, $SOD1^{WT}$, and non-Tg mice were gated on by CD11b expression. These microglia were analyzed for the proportion of CD11c+ cells, as shown on right. On left, cumulative analysis of day 135 non-Tg ($n = 6$), $SOD1^{WT}$ ($n = 5$), and $SOD1^{G93A}$ ($n = 14$) mice. Statistical comparison is by one-way ANOVA with Bonefferoni's post hoc test, ***, $P < 0.001$. On average, 68.66 ± 2.846% of microglia were positive for CD11c.

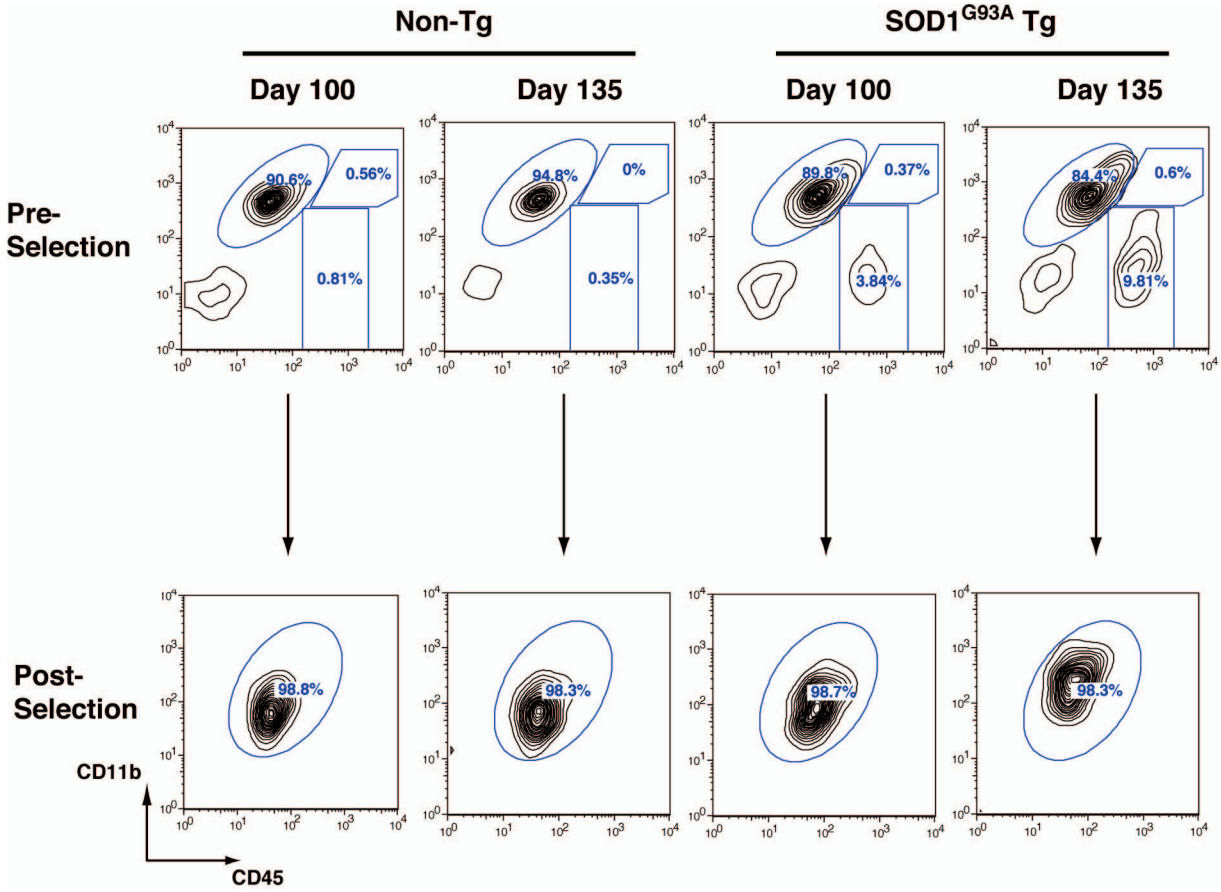

Fig. S6. CD11b magnetic bead selection of microglia. Microglia were purified from CNS percoll gradient isolated cells by magnetic bead selection. To determine the purity of microglia selection, cells pre and postselection were stained for CD11b and CD45. Representative samples from day 100 and day 135. SOD1^{G93A} (*Right*) and non-Tg (*Left*) mice are shown. Above. Preselection leukocytes contain CD11b- cells such as lymphocytes (CD11b-CD45hi). Below. Postselection, greater than 98% of cells are CD11b+ microglia. CD11b antibody staining decreases somewhat, likely because of competition with the magnetic CD11b selection beads.

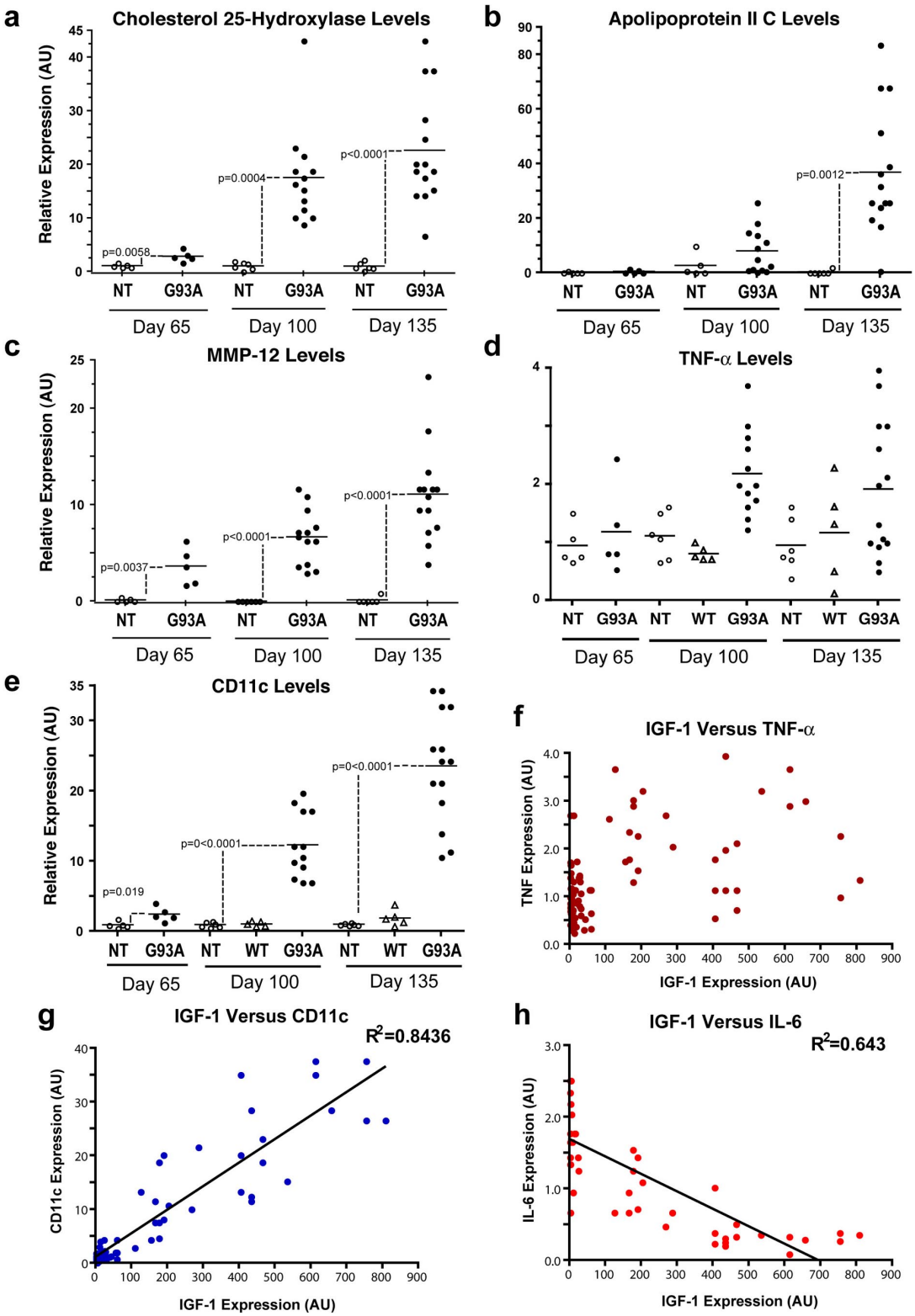

Fig. S7. Microglia gene expression profile shows a direct correlation of IGF-1 with CD11c expression and inverse with IL-6. Purified spinal cord microglia from SOD1^{G93A}, SOD1^{WT}, and Non-Tg mice were subjected to quantitative PCR for (*a*) Cholesterol 25-hydroxylase (*b*) Apolipoprotein II C (*c*) Matrix metalloproteinase 12 (d) TNF- α and (*e*) CD11c levels. Statistical analysis shows *p*-values, by *t* test. (*f–h*) IGF-1 expression levels (*x* axis) are plotted against TNF-α, CD11c and IL-6 levels (*y* axis). These expression levels were determined by qPCR previously. Regression lines with R^2 correlation values are shown.

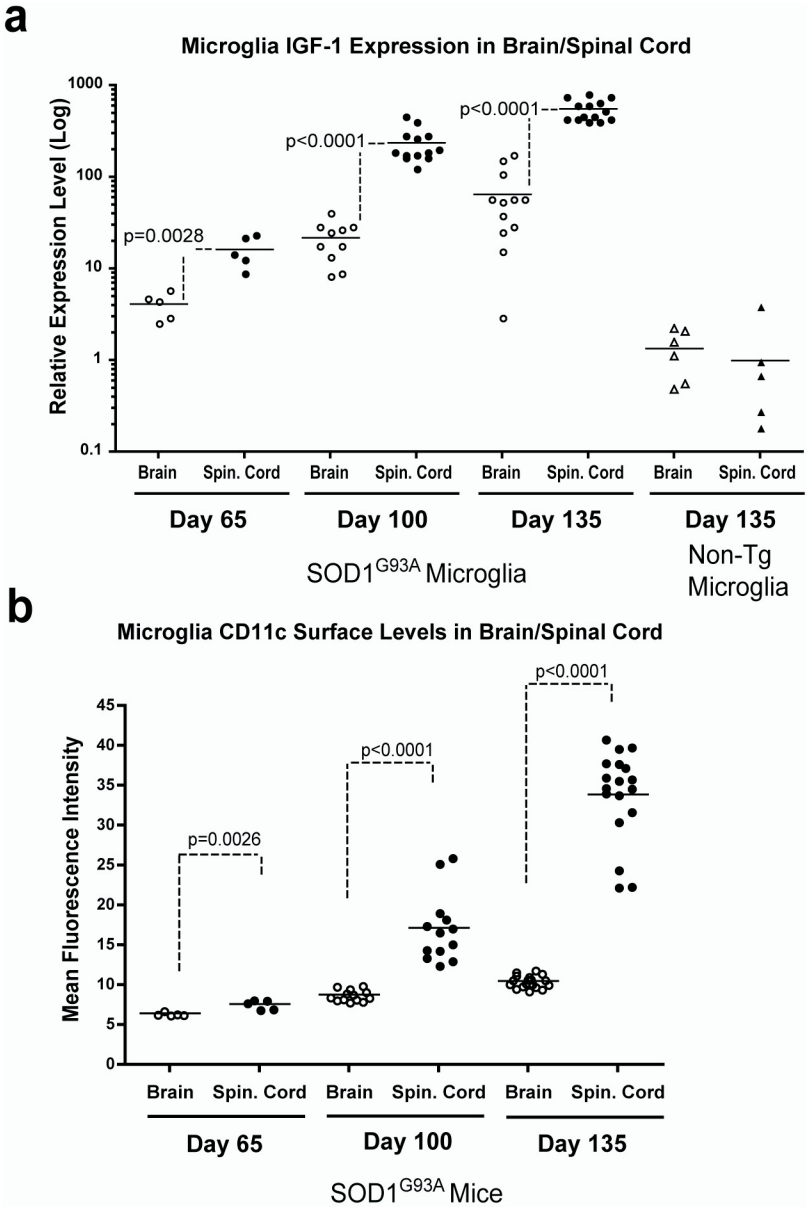

Fig. S8. Comparison of spinal cord and brain inflammation. Microglia show greater phenotypic changes in spinal cord than brain. (*a*) IGF-1 expression levels compared between magnetic bead purified spinal cord and brain microglia during disease progression (log scale). IGF-1 levels in purified microglia in non-Tg mice are shown on the right. (*b*) Surface levels of CD11c determined by flow cytometry on microglia from spinal cords or brains of $SOD1^{G93A}$ mice at day 65 (spinal cord, $n = 5$, brain, $n = 5$), day 100 (spinal cord, $n = 13$, brain, $n = 10$), and day 135 (spinal cord, $n = 14$; brain, $n = 12$).

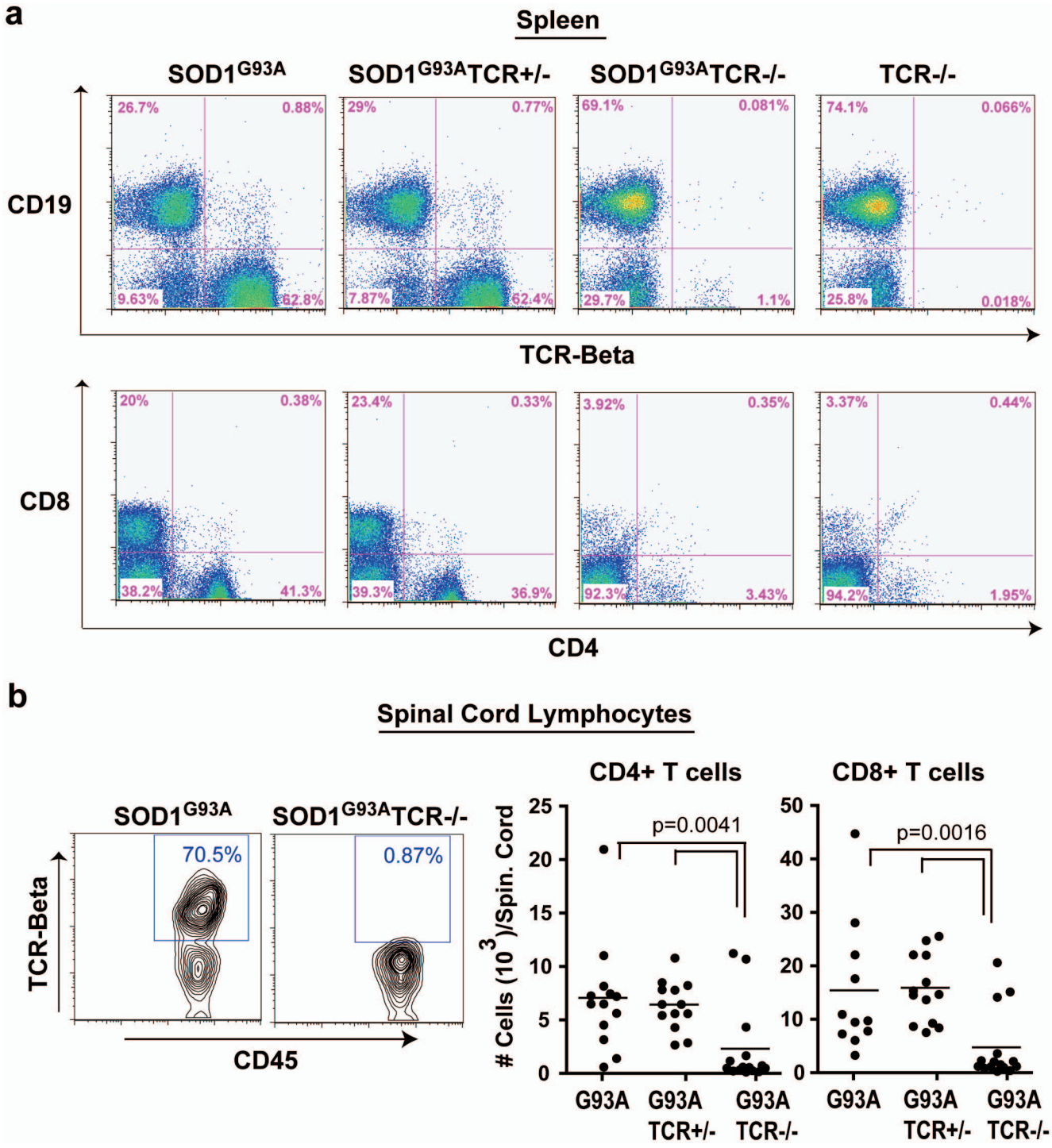

Fig. S9. Specific depletion of T lymphocytes in SOD1^{G93A}Tg TCRβ−/− mice. (*a*) Splenocytes from SOD1^{G93A}, SOD1^{G93A} TCR±, SOD1^{G93A} TCR−/−, and TCR−/− mice were stained for CD19+ B cells, TCRβ+ T cells, and CD4 or CD8+ cells. As shown, the TCRβ+, CD4^{+} and CD8+ T cell populations were depleted in SOD1^{G93A} TCR−/− mice, while the CD19+ B cell population remains intact. Numbers in quadrants indicate population percentages. (*b*) (Left) Spinal cord lymphocytes (CD11b+CD45hi) in SOD1^{G93A} and SOD1^{G93A} TCR−/− mice were analyzed for expression of TCRβ. (Right) Quantification of spinal cord CD4^{+} and CD8+ T cell populations in spinal cords of SOD1^{G93A} Tg, SOD1^{G93A} TCR±, and SOD1^{G93A} TCR−/− mice at end-stage. As shown, the majority of peripheral and CNS infiltrating T lymphocytes are depleted in SOD1^{G93A} TCR−/− mice.

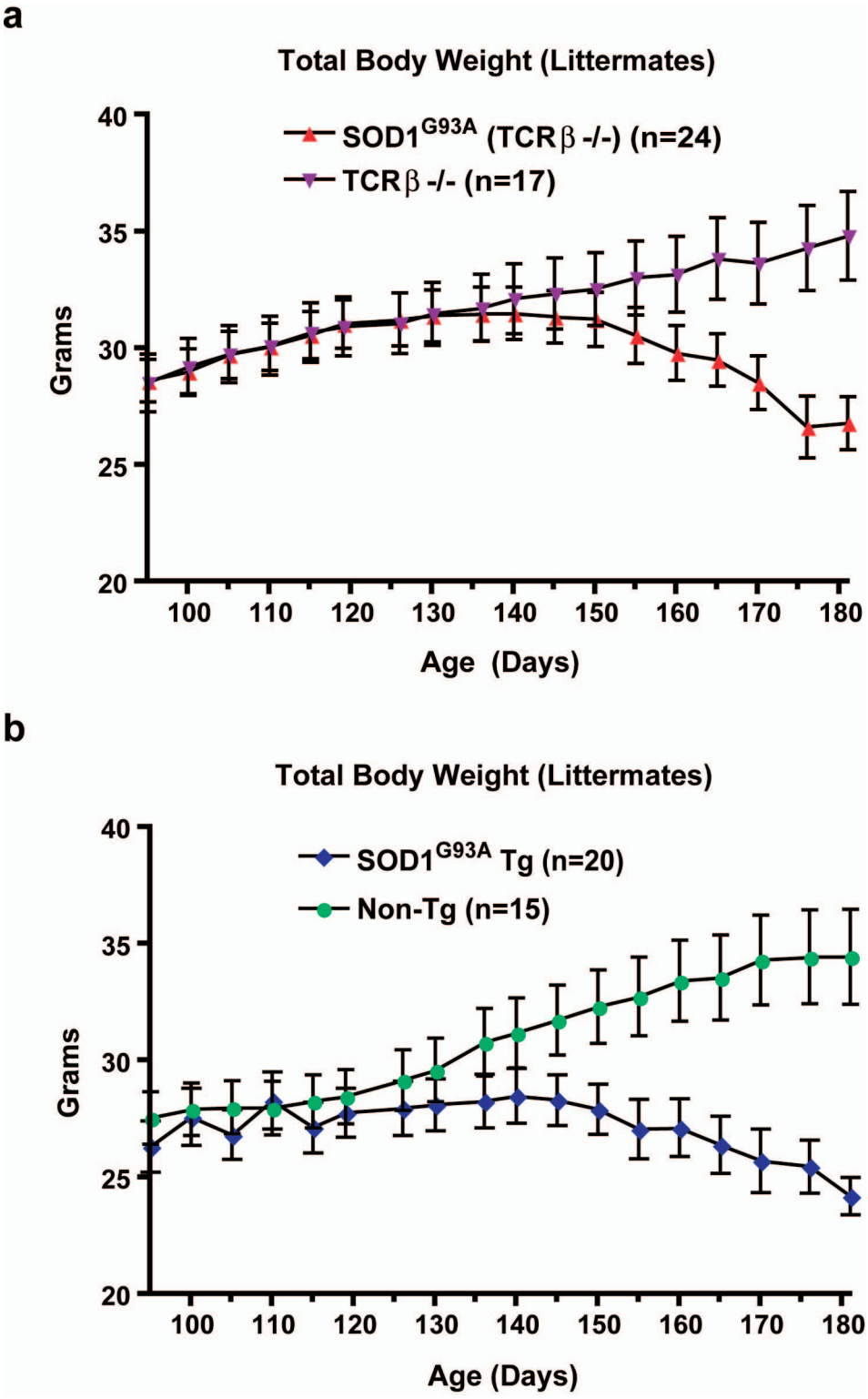

Fig. S10. Body weight changes during disease progression. Total body weight was measured and compared in (*a*) TCR$\beta-/-$ mice and SOD1^{G93A} TCR$\beta-/-$ littermates, (*b*) non-Tg mice and SOD1^{G93A} littermates. Error bars, SEM.

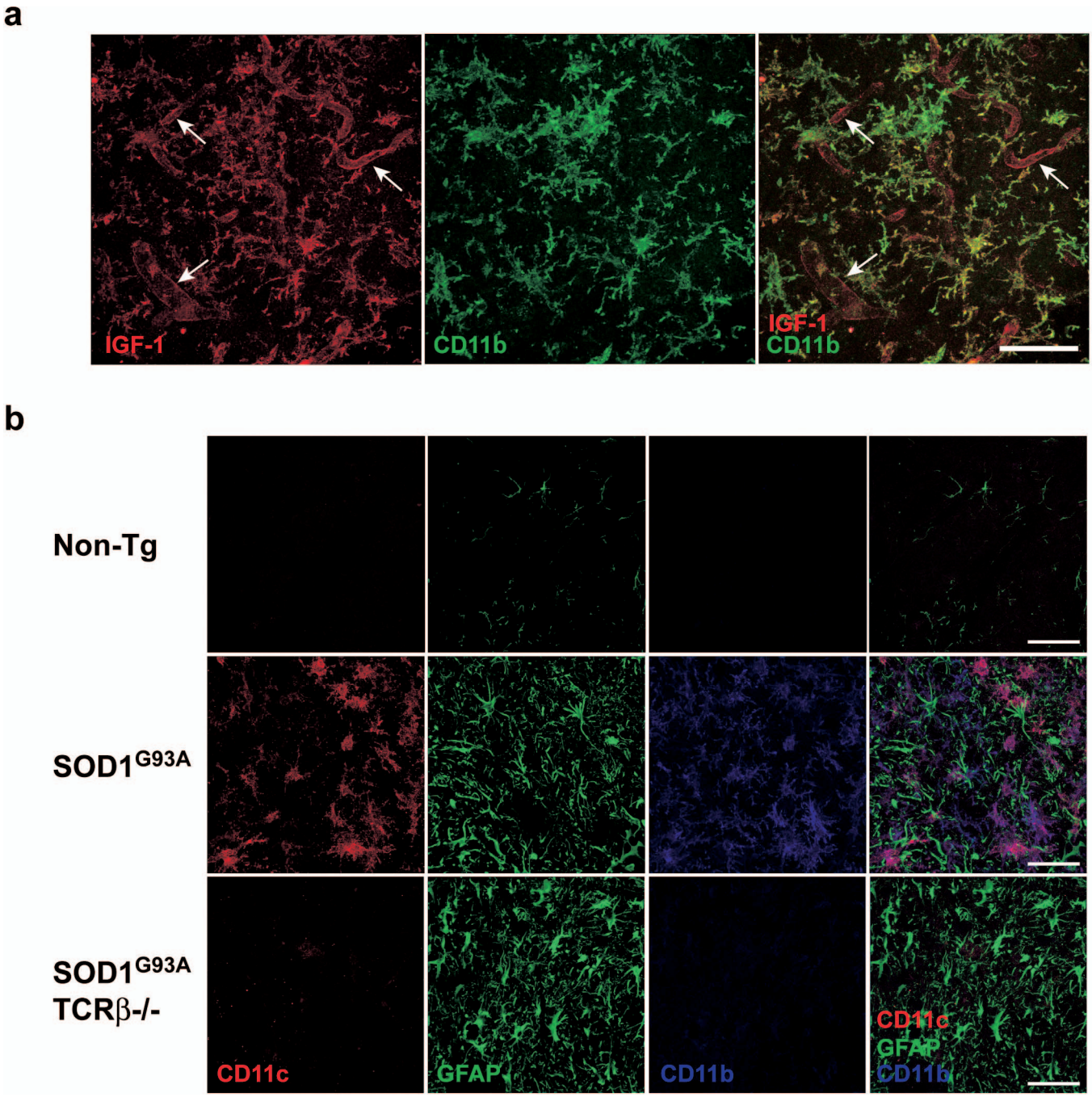

Fig. S11. IGF-1 is localized to microglia and blood vessels. CD11b+CD11c+ reactive microglia in mutant SOD1 mice are dependent on T lymphocytes. (*a*) Immunostaining for IGF-1 (red) and CD11b (green) in $SOD1^{G93A}$ Tg lumbar spinal cord sections. By confocal microscopy, IGF-1 is expressed by CD11b+ microglia and also present in blood vessels (white arrows). (Scale bar, 50 μm.) (*b*) Spinal cord sections were costained for CD11c (red), GFAP (green), and CD11b (blue). In $SOD1^{G93A}$Tg TCR$\beta-/-$ sections, microglia reactivity for CD11b and CD11c is reduced, while GFAP staining is unaffected. (Scale bar, 50 μm.)

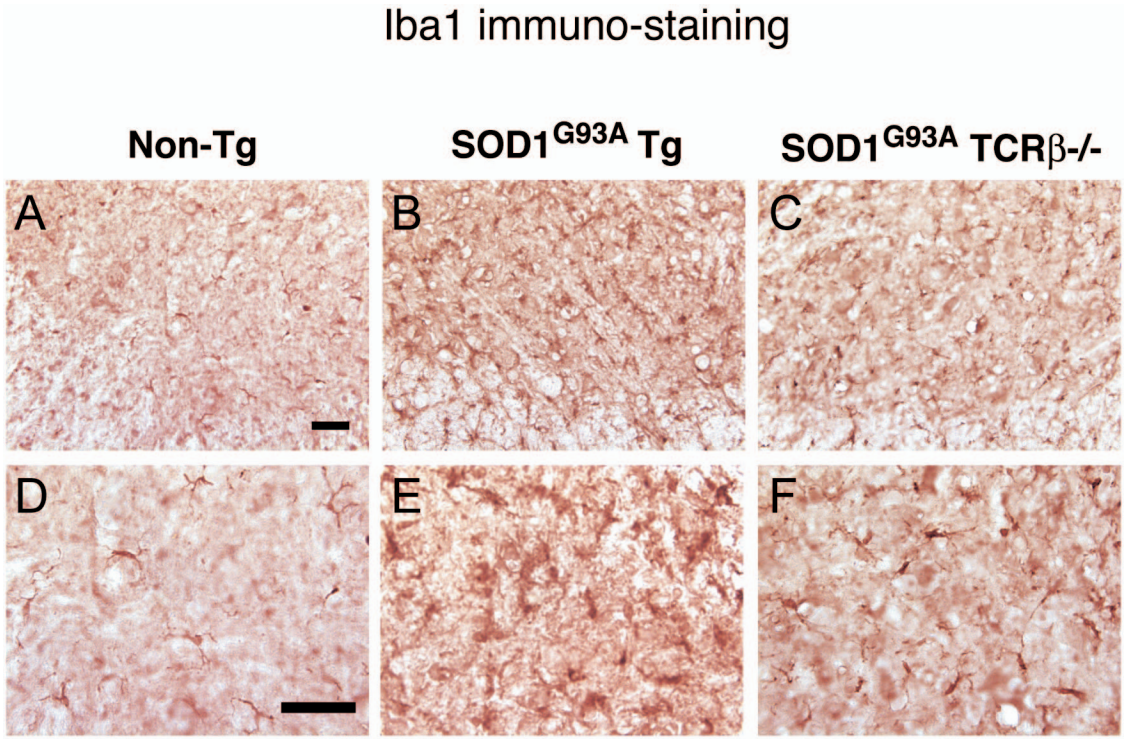

Fig. S12. Motor neuron loss is accelerated in SOD1^{G93A}Tg TCR$\beta-/-$ mice. (*a*) Representative Nissl stained neurons at day 140, end-stage, in ventral horn areas of Non-Tg, SOD1^{G93A}, and SOD1^{G93A} TCR$\beta-/-$ lumbar spinal cord. (*b*) Motor neurons counts were averaged over non-consecutive 30 μm sections of individual lumbar spinal cords. Mean $\pm$ SEM. motor neurons/mm^2 was determined for sets of animals ($n = 2–4$) at day 140 and end-stage (NT, non-Tg animals at end-stage are age-matched littermates of G93A mice).

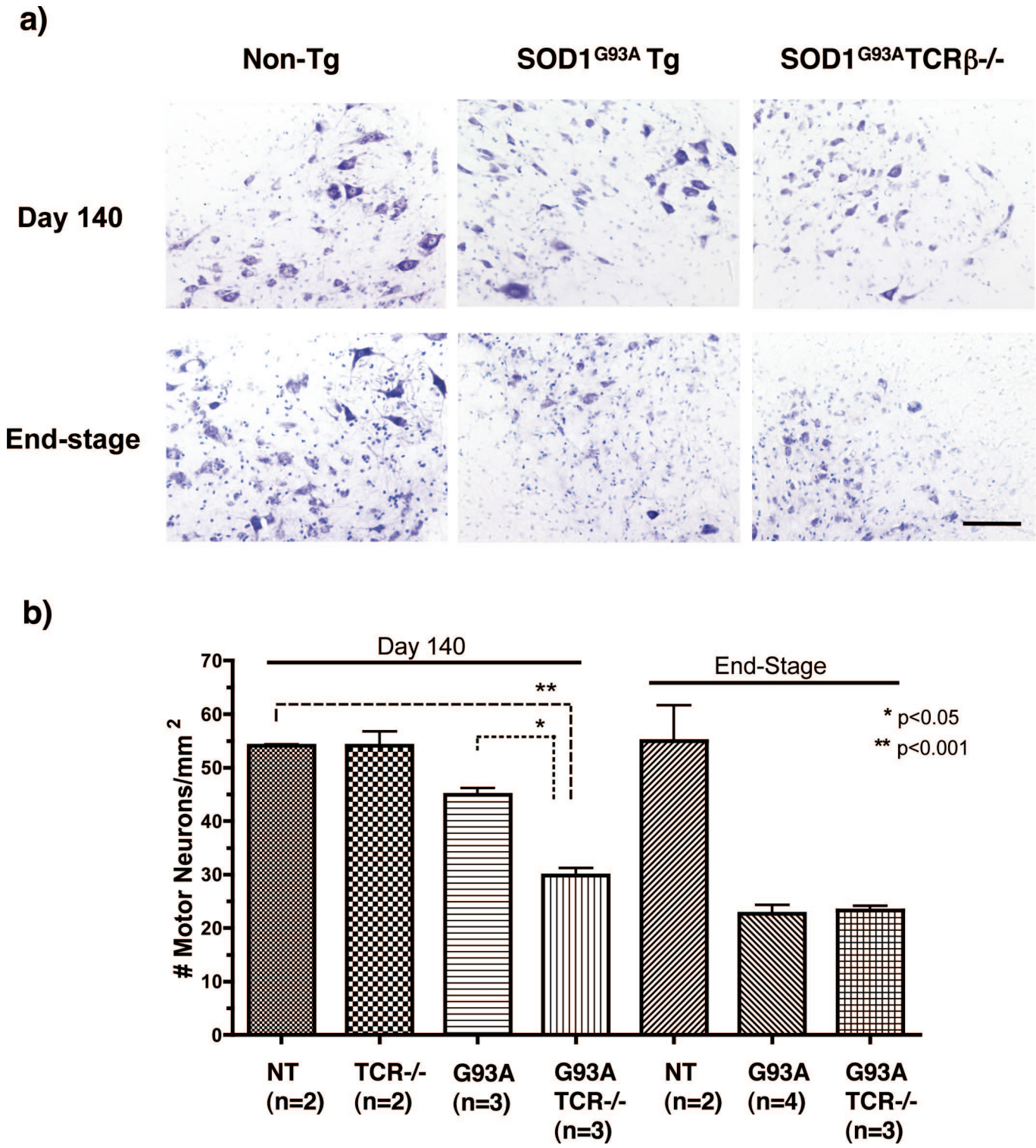

Fig. S13. Morphological activation of microglia is affected by absence of T lymphocytes. Spinal cord sections from Non-Tg control littermates (A, D), end-stage SOD1^{G93A} Tg (B, E), and SOD1^{G93A} TCR$\beta-/-$ (C, F) mice were stained for rabbit anti-Iba1 immuno-histochemistry. In SOD1^{G93A} Tg mice, microglia adopt amoeboid, hypertrophied morphology. This activation response is reduced in SOD1^{G93A} TCR$\beta-/-$ mice. (Scale bar, 50 μm.)

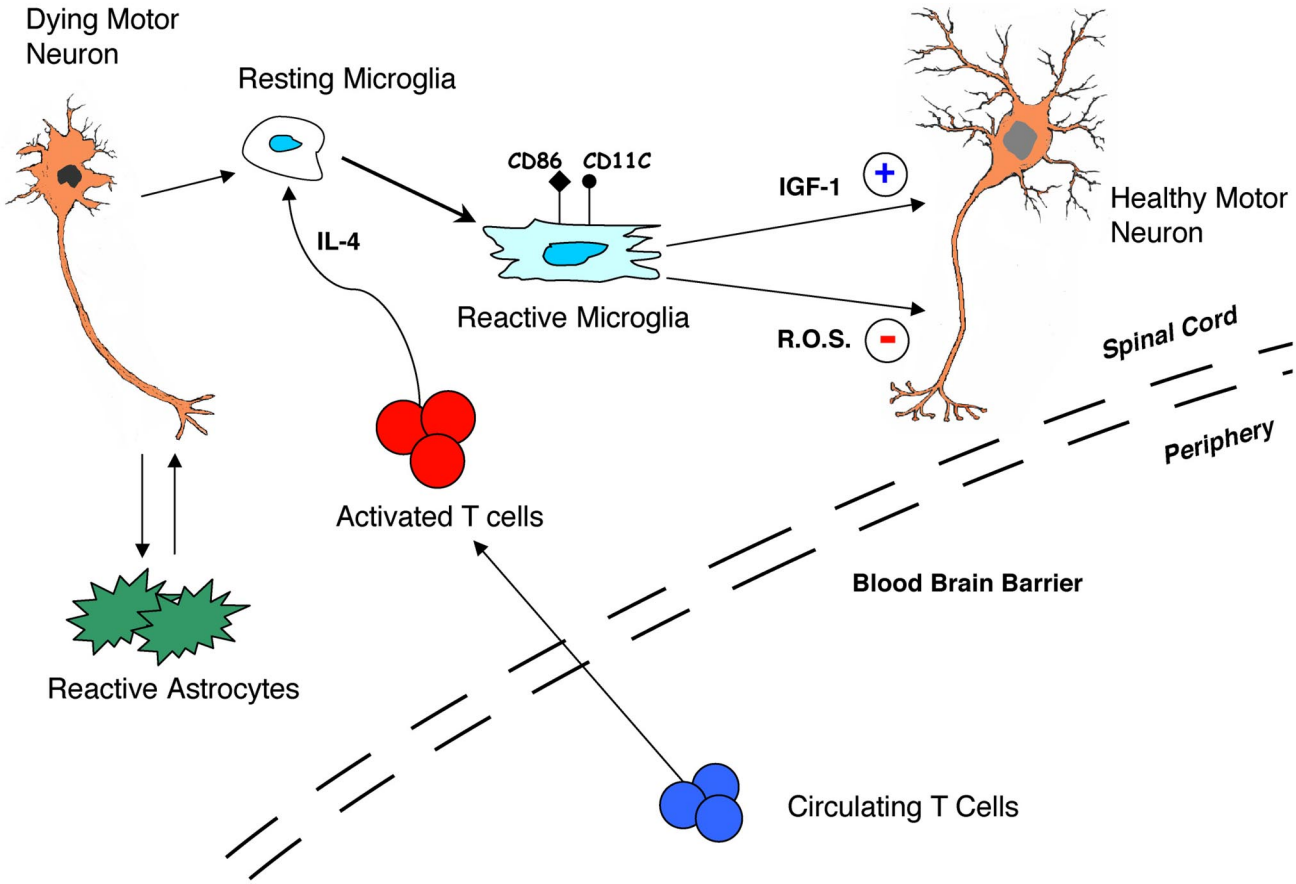

Fig. S14. Discussion Figure. Role of immunity in ALS. A proposed model for neuroinflammation in ALS is diagrammed. Dying motor neurons release signals which activate astrocytes and microglia. In conjunction, T cells are recruited from the periphery and secrete IL-4. Microglia up-regulate dendritic cell receptors CD11c and CD86, and interact with T cells. Microglia secrete both positive and negative factors to motor neurons; IGF-1 provides neuroprotection while reactive oxygen species has deleterious effects. Other unidentified factors from microglia may also contribute to neuronal survival.

Other Supporting Information Files

Table S1
Table S2
Table S3
Table S4
Table S5